6. BEAM DYNAMICS IN THE RF GUN

We have used three distinct computer simulation codes to model the behavior of the beam in the rf gun and the following beamline. HOMDYN [1] models the beam as a sequence of slices, with each slice propagated by a set of envelope equations. This code executes rapidly and may be used to model very long stretches of beamline. We use HOMDYN for initial parameter scans, to identify possible operating points. PARMELA [2] tracks particles in external fields via integration of the Maxwell-Lorentz equations of motion. Self-field effects are included in the electrostatic approximation, calculated in the beam's center-of-momentum frame. PARMELA has been used extensively to examine emittance growth in the rf gun and to further explore the possible operating points. MAFIA is a self-consistent electromagnetic solver that may track particles using a 2D relativistic particle-in-cell (PIC) module (TS2400). MAFIA simulations are intensive both in CPU cycles as well as in memory storage requirements. Hence, simulations with MAFIA are limited to exploring the detailed beam dynamics within the rf gun only, as a means of calibrating and benchmarking simulations with HOMDYN and PARMELA.

CROSS-CODE BENCHMARKING TESTS

We have produced simulations and comparisons between the codes by modeling the previously considered 3-cell rf gun [3]. The gun was simulated in each of the codes for a range of operating parameters. For simplicity, the beam is assumed to have rectangular profiles both in radius and in time, with uniform charge density. The spot size on the cathode has a radius of 2 mm, which represents a reasonable working point to balance initial thermal emittance with transverse space charge. For these initial tests to benchmark the codes, the thermal emittance was set to zero. The design goal is a geometric-averaged normalized emittance of 3 mm-mrad at the output of the gun. The bunch parameters are recorded after the first cell (z = 0.65 mm), and at the exit of the gun (z = 300 mm). In these simulations, a 3-cell model was used. The peak (on-axis) electric field in the first cell was 64 MV/m, while the second and third cells had peak fields of 43MV/m each.

Space-charge effects

The acceleration of a 20 psec (FWHM), 1 nC bunch represents a 50-ampere instantaneous current with significant space charge defocusing force. The codes have been used to analyze the transport from the cathode to the end of a 3-cell structure. In these simulations, only the external rf fields in the cavities were present, no solenoidal focusing was yet present.

To study the effects of space charge the parameters were varied in two ways. First, the charge within the bunch was varied from 1 pC to 1 nC keeping all other parameters fixed. Figure 6-1 shows how the normalized transverse emittance varied, indicating a clear blow up at high charge as expected from space charge effects. MAFIA and PARMELA agree quite well at the exit of the first cell (65 mm) but differ at the gun exit (300 mm).

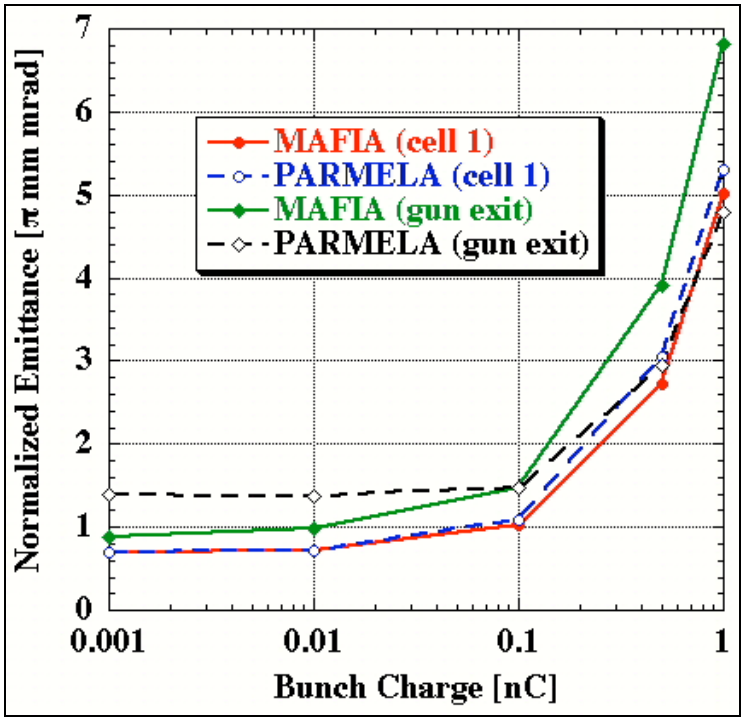

Figure 6-1 Variation of normalized transverse emittance with bunch charge, 64 MV/m on cathode, 60° launch phase, 10 ps bunch length, 43 MV/m for cells 2 and 3.

The other method kept the charge fixed at 1 nC and varied the bunch length from 10 ps to 40□s, thus reducing the charge density by up to a factor of four. Figure 6-2 shows how the transverse emittance from MAFIA varied over this range. Clearly there is less sensitivity to charge density in this case. At the end of the first cell (65 mm), the transverse emittance is seen to decrease monotonically with pulse length, as the longitudinal emittance increases linearly. That the longitudinal emittance increase linearly with pulse length in the early stages is expected since the energy spread has not yet had sufficient time to respond to longitudinal space charge or nonlinear rf forces. However, by the end of the rf gun, the effects due to increasing the bunch length become clearer. The transverse emittance shows a definite minimum as space charge forces lessen while nonlinear rf focusing increases. A similar trend is observed in the longitudinal phase space. The induced head-tail energy spread from space charge forces decreases with bunch length, while the nonlinear effects of the large rf phase range become more significant. However, we see that operation around the minima to decrease transverse emittance and space charge induced head-tail energy spread indicates a bunch length between 20 ps and 30□s.

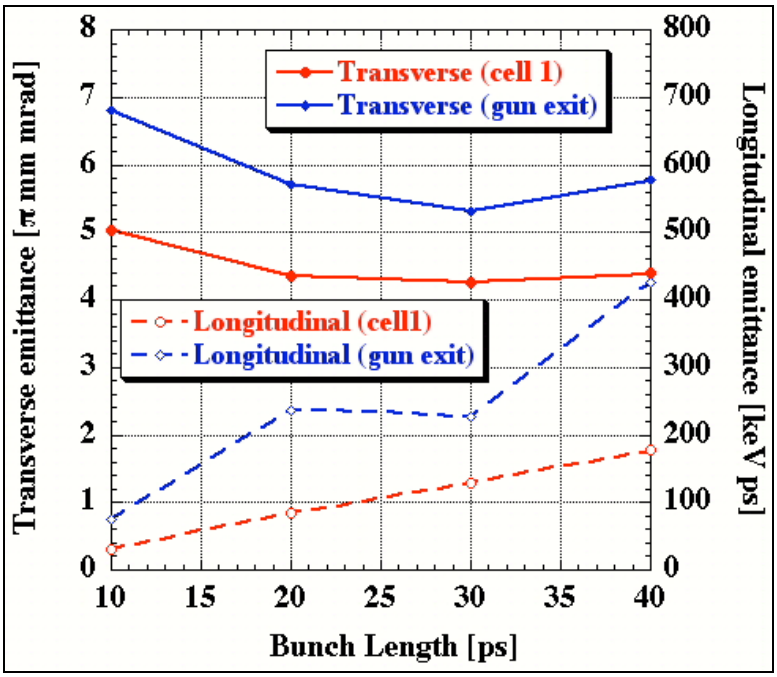

Figure 6-2 Variation of normalized transverse emittance with bunch length, 64 MV/m on cathode, 60° launch phase, 1 nC charge, 43 MV/m for cells 2 and 3 (MAFIA).

Launch phase

Another important parameter in the gun dynamics is the phase of the rf cycle at which the bunch is launched from the cathode. Simulations were run with launch phases from 10° to 90° with all other parameters fixed, see Figure 6-3. The optimum appears to be well ahead of crest. This may indicate that rf focusing is at least as important as accelerating field at the cathode.

Simulations show a similar trend in the longitudinal emittance after the first cell, although the codes differ on the final number. Bunching due to the slope of the rf waveform may be compensating for longitudinal space charge forces at low phase angle. The calculated longitudinal emittance leaving the last cell doesn't show a clear trend, however no attempt was made to optimize the relative phasing of the later cells for different launch phases.

Phase offset between first and second cells

Introduction of the short drift between the gun cell and the subsequent accelerating cells introduces a small timing offset. Retarding the downstream cells by about 30° can compensate this. However, simulations indicate that apart from a small increase in the energy there is not much effect on the output beam parameters when this is added.

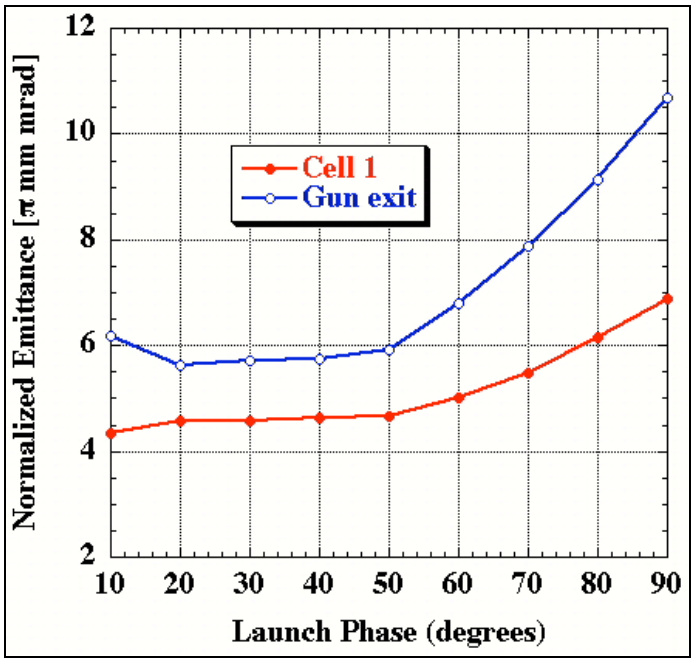

Figure 6-3 Variation of normalized transverse emittance with launch phase, 64 MV/m on cathode, 1 nC, 10 ps bunch length, 43 MV/m for cells 2 and 3 (MAFIA).

SOLENOID COMPENSATION OF EMITTANCE

Emittance compensation techniques have been thoroughly described in the literature [4,5]. Briefly, emittance compensation is the process by which the transverse phase space profiles of different *slices* along the bunch are made to re-align in a coherent way so as to reduce the sum, or *projected*, emittance of all the slices to its minimum value. This minimum value is bounded from below by the initial thermal emittance.

These techniques are employed to deliver the lowest possible transverse emittance at a specified point downstream from the exit of the rf gun. Typically, this point is made to coincide with the entrance of a subsequent accelerating structure. Shown in Figure 6-4 below is the result from a HOMDYN simulation of the 3-cell rf gun, without solenoidal focusing (uncompensated) and with solenoid coils excitation (compensated). In the compensated case, the solenoids have been tuned to produce a beam that exhibits very little projected emittance growth in the drift region nearly two meters past the end of the rf gun. This particular configuration does not generate the minimal normalized transverse emittance possible in the drift region. However, the very long beam waist achieved may be more beneficial for matching into a downstream skew quadrupole lattice. This issue is currently being considered.

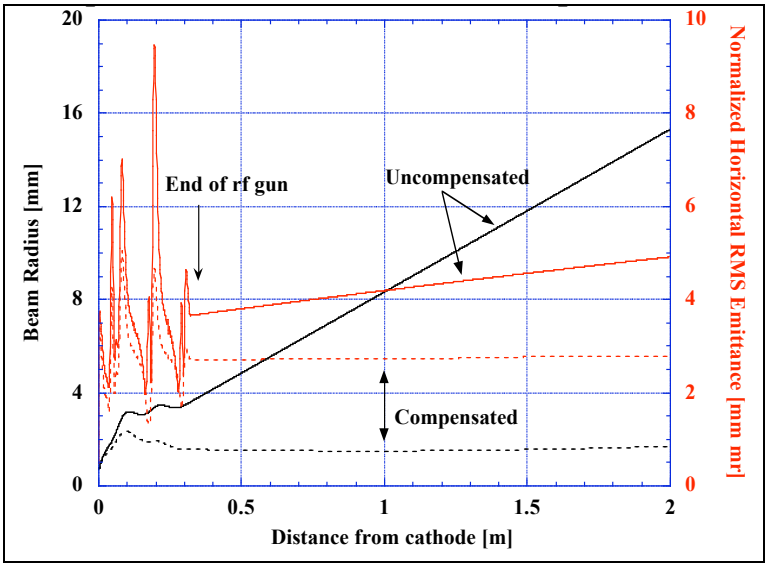

Figure 6-4 HOMDYN model of uncompensated (solid) and compensated (dashed) beam dynamics in the rf gun and drift section.

The flat beam photoinjector differs from previously studied rf photoinjectors in a fundamental way. Previous designs were concerned with propagating a beam through an azimuthally symmetric channel, at least as far as the exit of the pre-accelerators when space charge effects were no longer relevant to the detailed beam dynamics. Hence, symmetry was maintained until it no longer mattered. Actually, this is true for the majority of electron injectors, with the exception of sheet beam klystrons. For the proposed photoinjector, however, we must design a beamline that intentionally breaks the azimuthal symmetry by the introduction of skew quadrupoles in a region where space charge effects are still important. Moreover, while azimuthally symmetric photoinjectors strive to produce beams with emittances in both the horizontal and vertical planes of less than 1π mm-mrad for a 1 nC bunch charge, we need only produce a beam that has a geometric-averaged emittance of ~3π mm-mrad for a 1 nC bunch charge. However, we must do this while producing a high ratio (>50-100:1) between the horizontal and vertical emittances at the end of the injector. We must eventually produce a beam with vertical emittance approximately equal to the initial, thermal emittance value or less. Hence, our strategy for emittance compensation will differ in some respects from the already established technique.

THEORETICAL CONSIDERATIONS

Previous emittance compensation studies have assumed that the beam is emitted at a location free from magnetic fields, and that any contribution to the beam envelope due to canonical angular momentum is negligible. In this study, we intentionally apply a solenoid field such that lines of magnetic flux thread the cathode. The envelope equation describing the evolution along

the beamline, parameterized by distance (z), of the RMS radial beam spot size ($\sigma_r = \sqrt{\langle r^2 \rangle}$) can be expressed as [6]

$$\sigma_r'' + \left(\frac{\gamma'}{\gamma}\right)\sigma_r' + K_r\sigma_r - \frac{\sigma_s}{\sigma_r + \sigma_x} - \frac{\varepsilon_{nr}^2}{\sigma_r^3 \gamma^2 \beta^2} - \left(\frac{p_\theta}{mc\gamma\beta}\right)^2 \frac{1}{\sigma_r^3} = 0. \tag{1}$$

where the second term represents the focusing effect from acceleration. The third term multiplier, $K_r = \left(\frac{eB_z}{2\gamma\beta mc}\right)^2$, represents the influence of linear focusing in a solenoidal magnetic channel. The fourth term multiplier, $\sigma_s = 2I/I_0$, represents the defocusing influence of space charge effects, with $I_0 = 4\pi mc/\mu_0 e \approx 17kA$. The final two terms represent the defocusing influence of finite radial emittance and finite canonical angular momentum, which can be seen to influence the envelope dynamics in an equivalent manner.

The emittance term may be evaluated by several means [7]. In an azimuthally symmetric system, the total 4-D transverse emittance can be expressed as

$$\varepsilon_n^2 = \frac{1}{4}(\gamma\beta)^2\left[\langle r^2\rangle\langle r'^2 + (r\theta')^2\rangle - \langle r\cdot r'\rangle^2 - \langle r^2\theta'\rangle^2\right], \tag{2}$$

where $r' = dr/dz$, $\theta' = d\theta/dz$. This emittance represents the volume of the full 4-D transverse phase space and may be written in terms of the component emittances describing the radial and angular degrees of freedom,

$$\begin{aligned}\varepsilon_{nr}^2 &= \frac{1}{4}(\gamma\beta)^2\left[\langle r^2\rangle\langle r'^2\rangle - \langle r\cdot r'\rangle^2\right] \\ \varepsilon_{n\theta}^2 &= \frac{1}{4}(\gamma\beta)^2\left[\langle r^2\rangle\langle(r\theta')^2\rangle - \langle r^2\theta'\rangle^2\right].\end{aligned} \tag{3}$$

For rigid rotation (constant Γ), the last expression is identically zero. We may ignore the emittance in the angular degree of freedom, as this does not directly affect the evolution of the beam envelope until the beam enters the skew quadrupole channel.

The equation of motion for the angular degree of freedom of each particle can be expressed as the rate of the Larmor phase angle advance

$$\theta' = \frac{p_\theta}{\gamma\beta mcr^2} + \frac{eB_z}{2\gamma\beta mc}. \tag{4}$$

In the absence of canonical angular momentum, the Larmor phase angle advances at one-half the rate of cyclotron phase angle.

This last expression is important to consider for the flat beam injector. The conditions at the cathode plane present initial conditions for the solution of this equation of motion. In the case of a typical injector, the magnetic field is designed to be null at the cathode plane. For this case, $B_z(z=0) = B_{z0} = 0$. From knowledge of the initial conditions at the cathode, we know that $\dot{\theta}(z=0) = \beta c\,\theta'(z=0) = 0$ and, hence, $p_\theta(all\ z) = 0$. This last relation follows from global

conservation of angular momentum. In the case of the flat beam injector, a finite magnetic field is required at the cathode plane. The conserved angular momentum for a particle emitted at radius r_0 is then

$$p_\theta = -\frac{1}{2} e B_{z0} r_0^2 . \tag{5}$$

The angular equation of motion determines the trajectory of beam particles in the angular phase-space. It depends upon the local particle radius, to which it is coupled by any finite canonical angular momentum. However, the radial envelope equation (as well as the individual particle's radial equation of motion) does not depend on the detailed evolution of the angular degree of freedom, so long as the beam remains azimuthally symmetric. This will be the case for the beams under consideration here, until they reach the entrance of the skew quadrupole transformer.

The radial envelope equation above describes the evolution of the radial degree of freedom of the ensemble of particles comprising the beam. The initial angular momentum contributes to the evolution of the beam envelope in the same way as the emittance. The effective radial emittance is then the sum in quadrature of the radial emittance (ε_{nr}) and the influence of the canonical angular momentum [7],

$$\varepsilon_{nr}^{eff} = \sqrt{(\varepsilon_{nr})^2 + \frac{1}{4}\left\langle \frac{p_\theta}{mc} \right\rangle^2} . \tag{6}$$

We may then study solutions to the envelope equation in the context of the design of the proposed rf gun by parameterizing with respect to the initial angular momentum. The rf gun design may then be considered optimized for a particular value of the initial angular momentum when the effective radial emittance is minimized. For the eventual generation of flat beams with large emittance ratio, we will see that large values of the angular momentum are required along with preservation of the radial emittance to values close to that of the initial thermal emittance.

LARGE AND SMALL ANGULAR MOMENTUM REGIMES

We have used the HOMDYN code to evaluate possible operating points of the flat beam injector. These operating points are defined by the set of parameters: solenoid coil excitations (solenoid tune), laser spot size at the cathode. For the proposed 4-cell, 5-solenoid rf gun, this presents a 6-D parameter space. The set of solenoid coil excitations define the solenoid magnetic field at the cathode, and the cyclotron phase advance once the rf fields and beam launch phase are given. The laser spot size at the cathode determines the thermal emittance, the canonical angular momentum (once the solenoid field at the cathode is known), and provides the starting point for solution of the envelope equation and for calculating the Larmor phase advance. By searching the available parameter space, we can make some initial predictions of the performance of the rf gun portion of the injector.

For any set of solenoid fields used, the degree of emittance compensation provided by solenoid focusing can be measured against the cyclotron phase advance θ_c, defined by

$$\theta_c\left(t_{final}\right) = \int_0^{t_{final}} dt \frac{eB_z}{m\gamma}. \tag{7}$$

This parameter is only useful when comparing simulations or experimental data sets when the laser spot size incident on the photocathode is held constant from one case to another. In the general case where the spot size is also allowed to vary, the more general Larmor phase advance given by

$$\theta_L\left(t_{final}\right) = \int_0^{t_{final}} dt \left(\frac{p_\theta}{m\gamma}\frac{1}{r^2} + \frac{eB_z}{2m\gamma}\right) \tag{8}$$

is more appropriate. The utility of the cyclotron phase advance is such that it only depends on the solenoid tune and the beam energy. It provides a measure independent of the beam envelope dynamics, including space charge and emittance effects.

Below we present results that have been parameterized by the initial angular momentum in units of emittance (π mm-mrad). These simulations show the solution of the envelope equation of the beam as it is emitted from the cathode, passes through the rf gun, and exits the region of solenoid field to the drift section beyond. We do not consider the skew quadrupole channel here, except to match the beam envelope to the entrance of the channel located approximately 1 m from the cathode plane (z = 0 m).

At the cathode plane, the thermal emittance is determined by the product of the laser spot size with the distribution of the transverse electron momenta,

$$\varepsilon_{nr}^{thermal} = \frac{1}{2}(\beta\gamma)_{cathode}\sqrt{\left\langle r^2\right\rangle_{cathode}\left\langle r'^2\right\rangle_{cathode}}\,. \tag{9}$$

For Cs_2Te cathodes, HOMDYN uses an analytic model [8] for the thermal emittance, approximately 0.7π mm-mrad per mm of initial rms beam radius.

We have identified two regimes of operating points. The first regime occurs for small values of angular momentum (< ~15π mm-mrad) and thermal emittance (~0.7π mm-mrad). A typical solution (with angular momentum contribution ~8π mm-mrad) is shown in Figure 6-5. This regime can achieve optimized solutions that demonstrate radial emittance ~3π mm-mrad and very long beam waists. While the radial emittance has grown to several times that of the initial thermal value, it still remains within the design specifications. The beam envelope and radial emittance remain relatively constant over nearly 2 m of drift, which may be advantageous for matching into the flat beam adapter lattice.

The second regime occurs for larger angular momentum (~20-50π mm-mrad), and larger thermal emittance (~1-2 π mm-mrad). This regime is characterized by larger spot sizes (up to ~3 mm rms radius) to generate the larger initial angular momenta, and overall larger excitation of the focusing solenoids. The results of two optimized solutions in this regime are presented in Figure 6-6. The resulting envelope solutions show minima in radial emittance at the adapter entrance (z ~ 1 m) that exhibit only small growth (~10%) above the initial thermal emittance value.

These two simulations demonstrate the feature of emittance oscillation and compensation. Both simulations demonstrate the radial emittance undergoing oscillations. The first of the minima is located at the cathode (z = 0 cm), with the next local minima located (by careful optimization of the solenoid focusing channels) approximately 1 m from the cathode.

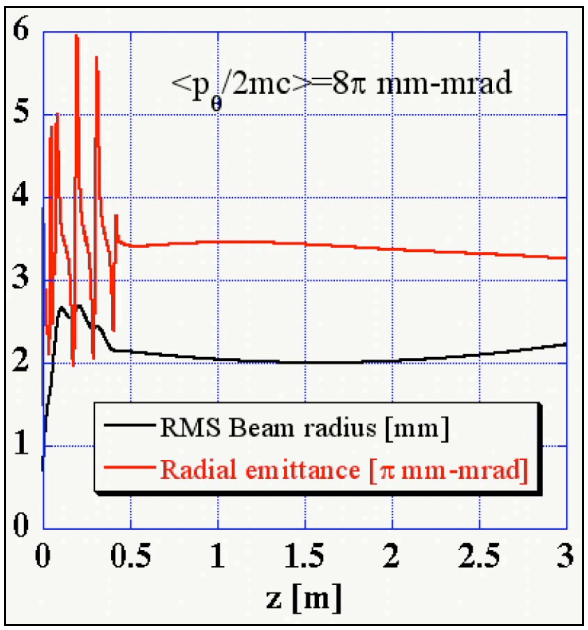

Figure 6-5 Small angular momentum regime (HOMDYN).

These solutions may be more suitable for the flat beam injector, provided they can be matched into the skew quadrupole channel. We will consider working points in the large angular momentum regime below when we discuss the initial design of the flat beam adapter for the proposed injector.

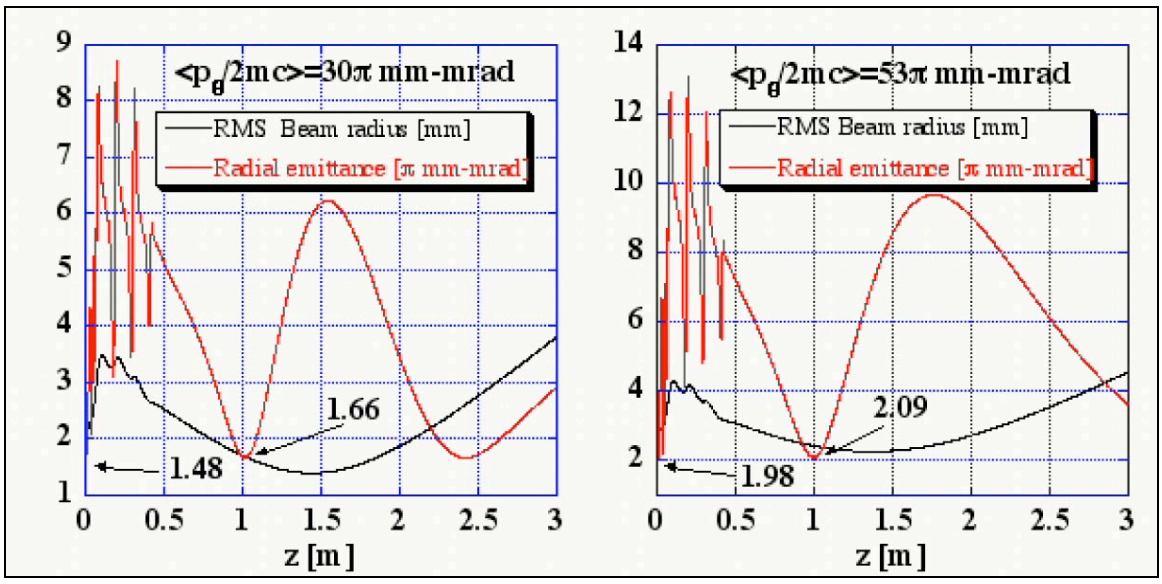

Figure 6-6 The initial thermal emittance and the projected emittance at the adapter entrance are indicated (HOMDYN)for the large angular momentum regime.

REFERENCES

[1] M. Ferrario, *et al.*, 'Multi-bunch energy spread induced by beam loading in a standing wave structure', Particle Accelerators, **52**, 1 (1996).

[2] L. Young and J. Billen, PARMELA code manual, LANL Report No. LA-UR-96-1835 (Revised), 2002.

[3] R. Rimmer, *et. al.*, 'A High-Gradient, High-Duty-Factor rf Photo-Cathode electron Gun', to appear in the Proceedings of the Eighth European Particle Accelerator Conference (EPAC 2002), Paris, France, 2002.

[4] B.E. Carlsten, Nucl. Instrum. Methods Phys. Res. A **285**, 313 (1989).

[5] L. Serafini and J.B. Rosenzweig, 'Envelope analysis of intense relativistic quasilaminar beams in rf photoinjectors: A theory of emittance compensation', Phys. Rev. E, **55**, 7565 (1997).

[6] M. Reiser, Theory and Design of Charged Particle Beams (Wiley, New York, 1994).

[7] S. Nagaitsev and A. Shemyakin, 'Beam emittance calculation in the presence of an axially symmetric magnetic field', FERMILAB-TM-2107, 2000.

[8] K. Flöttmann, 'Estimation of the thermal emittance of electrons emitted by Cesium Telluride photo cathodes', TESLA-FEL-97-01, DESY-Hamburg, 1997.